

# Enhancing Computational Efficiency in Multiscale Systems using Deep Learning of Coordinates and Flow Maps

Asif Hamid<sup>a</sup>, Danish Rafiq<sup>a</sup>, Shahkar Ahmad Nahvi<sup>a</sup>, Mohammad Abid Bazaz<sup>b</sup>

<sup>a</sup>Department of Electrical Engineering, Islamic University of Science and Technology, Awantipora, 192122, Jammu & Kashmir, India

<sup>b</sup>Department of Electrical Engineering, National Institute of Technology, Srinagar, 190006, Jammu & Kashmir, India

---

## Abstract

Complex systems often show macroscopic coherent behavior due to the interactions of microscopic agents like molecules, cells, or individuals in a population with their environment. However, simulating such systems poses several computational challenges during simulation as the underlying dynamics vary and span wide spatiotemporal scales of interest. To capture the fast-evolving features, finer time steps are required while ensuring that the simulation time is long enough to capture the slow-scale behavior, making the analyses computationally unmanageable. This paper showcases how deep learning techniques can be used to develop a precise time-stepping approach for multiscale systems using the joint discovery of coordinates and flow maps. While the former allows us to represent the multiscale dynamics on a representative basis, the latter enables the iterative time-stepping estimation of the reduced variables. The resulting framework achieves state-of-the-art predictive accuracy while incurring lesser computational costs. We demonstrate this ability of the proposed scheme on the large-scale Fitzhugh Nagumo neuron model and the 1D Kuramoto–Sivashinsky equation in the chaotic regime.

**Keywords:** Multiscale modeling, Deep learning, Data-driven modeling, Large scale systems, Scientific computing

---

## 1. Introduction

In the field of computational sciences and scientific computing, the numerical solution of partial differential equations (PDEs) is essential for understanding complex physical phenomena across a diverse range of disciplines, from fluid dynamics and electromagnetism to structural mechanics and quantum physics [1, 2]. However, complex PDEs often exhibit strong nonlinear behavior that makes it difficult or impossible to obtain analytical closed-form solutions. Therefore, numerical techniques are commonly employed to obtain approximate solutions of PDEs. For instance, the finite element analysis (FEA) [3] or the finite difference methods (FDM) [4] are used to approximate the derivative term in the PDEs by discretizing the spatial domains of interest into a grid or mesh. However, a fine discretization on complicated boundaries results in a large system of ordinary differential equations (ODEs) that can be computationally expensive to simulate. Additionally, PDEs governing physical laws often exhibit a multiscale nature, i.e., their behavior evolves on multiple distinct timescales that further increase the computational costs during numerical solutions [5]. A common situation is when two FEA models of different scales exist. In this case, evaluating a single element or time step of the large-scale FEA model requires at least one full simulation of the small-scale FEA model. This incurs extensive runtimes and significant computational costs.

While the computational costs for such systems remain high, their online evaluations are a major concern in many scientific and engineering applications requiring many system evaluations within a *many-query* framework. Some prominent applications include parameter and design optimization [6], multi-objective optimization [7], uncertainty propagation [8], high-throughput computing [9], and reinforcement learning (RL) [10, 11]. Even though expensive computational simulations are essential to resolve all the relevant scales, the important quantities of interest can be frequently characterized by a coarse-grained or average behavior [12]. However, determining the appropriate degree of freedom for such coarse-grained representations has always been challenging. As a result, various research efforts have been put into developing appropriate combinations of coarse-grained and fine-scale simulations that can accelerate the intense simulations at a controlled accuracy. Prominent hybrid methods include the equation-free framework (EFF) [13, 14], the heterogeneous multiscale method (HMM) [15], and the flow averaged integrator (FLAVOR)

method [16]. These methods distinguish between a fine (*micro*) scale, which is expensive to simulate, and a coarse (*macro*) scale. While EFF and HMM use coarse time steppers to simulate the evolution of macroscopic variables through a microscopic simulation, the FLAVOR method uses averaging flows to study the behavior. However, the accuracy of these methods is highly dependent on the separation of time scales, the time integrator used, and how well the information is captured at each scale. In addition to these methods, the classical *Fourier* and wavelet-based techniques can easily separate the coarse-grain and fine-grain features in both space and time [17]; however, these methods focus on identifying exclusively temporal or exclusively spatial coherence, which restricts their use for discovering models and predicting system states directly from data [18]. Nevertheless, these techniques are highly used and serve as the mathematical foundation of multiresolution analysis (MRA) [19].

Recently, there has been growing interest in predicting the multiscale behavior of systems directly from observational data using data-driven methods based on machine learning (ML) [20]. In this direction, various neural network-based schemes have been employed to forecast the solution of a multiscale system. For instance, ML methods have been used for various applications such as modeling dynamical systems [21, 22, 23, 24], in mesoscopic material modeling [25], in biological systems [26, 27], and in molecular kinematics, [28, 29]. The EFF framework has been extended with ML algorithms that learn the time interrogators and the transfer operators in an equation-free manner [30, 31]. In addition, sparse regression algorithms have been proposed to discover *Poincare* maps for multiscale problems [32] to discover slow timescale dynamics from signal exhibiting multiscale timescales [12]. Besides, the idea of learning a flow map of dynamical systems using neural networks [33, 34, 35] has been extended to multiscale problems in [36], wherein a novel multiscale hierarchical time-stepping (HiTS) method has been proposed. In particular, the authors have suggested using a hierarchy of neural network time stepper (NNTS) models that are trained at different time steps and then coupled for multiscale purposes. However, as we will show in this paper, the multiscale HiTS framework potentially suffers from huge computational expenses for systems governed by PDEs.

Thus, the aim of the paper is two-fold: (i) to discover a coordinate system in which the underlying dynamics of multiscale signals can be represented accurately on a few representative bases, and (ii) to provide a time-stepping scheme that marches the reduced coordinates forward in time. While we apply deep autoencoders (AEs) to accomplish the former goal, we make use of the multiscale HiTS estimation process to achieve the latter goal. In this way, we extend the applicability of the multiscale HiTS method to PDEs. Thus, the proposed method of *latent hierarchical time-stepping* (L-HiTS) learns an end-to-end mapping that accurately yet efficiently predicts the multiscale behavior of the PDEs from data. Although the multiscale HiTS scheme has been demonstrated for PDEs [36], the need for real-time applications and tasks for non-stationary dynamics calls for more efficient computations that the proposed scheme intends to address. The result is that the L-HiTS method maintains the same accuracy level as the multiscale HiTS method while providing significant computational speedups. To summarize, the key contributions of this paper are as follows:

1. We present a novel data-driven time-stepping scheme for systems governed by time-dependent PDEs involving multiscale physics. The proposed L-HiTS method is based on the joint discovery of the coarse-grained variables and flow maps inside the latent space, allowing for parallelization.
2. The L-HiTS scheme incurs lesser computational costs both at the training stage and testing stage than the multiscale HiTS method while delivering state-of-the-art prediction accuracy.
3. We demonstrate the applicability of the L-HiTS scheme for systems exhibiting multiscale and chaotic behaviors, representing real-world phenomena.
4. To make our work more accessible, we have provided open-source Python scripts that can be used to reproduce the results.

The remainder of the manuscript is as follows. In Section 2, we briefly introduce the multiscale analysis for predicting the solution of PDEs in a data-driven fashion. Next, in Section 3, we present how deep AEs can be used to learn a coordinate transformation that represents the actual dynamics onto a latent space and then how the existing multiscale HiTS scheme can be implemented in this latent space to achieve the task of prediction. We describe the idea and present a numerical algorithm. Thereafter, in Section 4, we show the application of the proposed scheme on two canonical PDEs. Finally, in Section 5, we discuss the sensitivity analysis for different choices of network parameters and present the conclusion of the study along with some drawbacks of the method that can be taken up in a future study.

## 2. Problem setup

This section provides an overview of the general methodology for predicting multiscale PDEs. To proceed with the idea, consider a nonlinear, continuous-time, multiscale dynamical system of the form:

$$\mathbf{u}_t = \mathcal{N}(\mathbf{u}, \mathbf{u}_x, \mathbf{u}_{xx}, \dots, \mathbf{x}), \quad (1)$$

where  $t$  is the time  $\in [0, T]$ ,  $x \in [0, n]$  is the spatial variable and  $\mathcal{N}(\cdot)$  is the nonlinear function of  $\mathbf{u}(x, t)$  and its derivatives. Using spatial discretization schemes such as the FEA, FDM, or the spectral method [3], the PDE system (1) can be approximated by a system of ODEs given by:

$$\dot{\mathbf{x}}(t) = \mathcal{N}(\mathbf{x}(t; \boldsymbol{\mu})), \quad \mathbf{x}(t_0) = \mathbf{x}_0, \quad (2)$$

where  $\mathbf{x} \in \mathbb{R}^n$  of dimension  $n$  represents the state vector, and  $\boldsymbol{\mu} \in \mathbb{R}^p$  denotes the system parameters, such as varying initial or boundary conditions. For a fine discretization,  $n$  is typically high, resulting in a large-scale initial value problem to be solved. Traditionally, the time solution of the ODE system (2) is obtained by employing different time-stepping integration schemes, including the explicit/implicit, fixed/adaptive, and one-step/multi-step methods with varying degrees of stability [37]. These numerical methods take successive time steps  $\Delta t$  into the future in an iterative manner to construct the discrete solutions for  $x(t)$ . Given the initial condition  $\mathbf{x}(t_0)$ , these methods approximate the discrete-time flow map

$$\mathbf{x}(t + \Delta t) = \mathcal{N}(\mathbf{x}(t), \Delta t) \triangleq \int_{\tau=t}^{t+\Delta t} \mathcal{N}(\mathbf{x}(\tau), \tau) d\tau, \quad (3)$$

usually via the *Taylor-series* expansion [38, 39, 40]. However, the accuracy of these methods depends upon the local step size  $\Delta t$  employed during the integration, making such time discretization local in nature. For instance, the classical *ode45* method uses a fixed-step, fourth-order *Runga-Kutta* scheme that incurs a local truncation error of  $\mathcal{O}(\Delta t^5)$  at every step of the solution and a global truncation error of  $\mathcal{O}(\Delta t^4)$ . In contrast, neural networks-based time-stepper models like those in [36, 33] learn a discrete flow map  $\mathcal{N}(\cdot)$  directly that progresses the state variables forward in time without being restricted by local step size limitations. Of the various neural network architectures available, residual neural networks (ResNets) are commonly used because they have lesser training times and work similar to that of a fixed-step, first-order *Euler's* scheme (see, e.g., Refs. [41, 33, 42, 43]).

ResNets are a special class of deep neural networks constructed by stacking multiple residual blocks [43]. Each residual block comprises simple feedforward layers that include identity skipped connections, allowing information to bypass the residual layers (cf. Figure 1). ResNets have been shown to outperform traditional feedforward neural networks (FNNs) in some applications, particularly in computer vision and image classification tasks [43]. The key advantage of ResNets is that they address the issue of vanishing gradients, a common problem in deep FNNs [33]. ResNets incorporate the identity operator into the network to have the network effectively estimate the residual of the input-output mapping. The ResNet block comprises  $L$  hidden layers, along with an identity operator that adds the input  $\mathbf{x}(t)$  back into the output. The architecture describes the following mapping;

$$\mathbf{x}(t + \Delta t) = \mathbf{x}(t_0) + \mathcal{N}(\mathbf{x}(t); \mathbf{W}), \quad \mathbf{x}(t_0) = \mathbf{x}_0, \quad (4)$$

where  $\mathbf{W}$  represents the weights of the neural networks, and  $\mathcal{N}(\cdot; \mathbf{W}) : \mathbb{R}^n \rightarrow \mathbb{R}^n$  is the nonlinear flow map learned by the network given as:

$$\mathcal{N}(\mathbf{x}(t); \mathbf{W}) = \mathbf{a}_L(\mathbf{W}_L(\dots \mathbf{a}_1(\mathbf{W}_1) \dots)), \quad (5)$$

where  $a_k$  ( $k = 1, \dots, L$ ) is the activation function used at layer  $k$ , and  $W_k$  corresponds to weights for the  $k^{\text{th}}$  layer. The weights are obtained by minimizing the *prediction* loss function  $\mathbf{W}_{pred}^*$  given as:

$$\mathbf{W}_{pred}^* = \arg \min_{\mathbf{W}} \frac{1}{p \times T} \sum_{i=1}^p \sum_{j=1}^T [\mathcal{L}_{pred}(\hat{\mathbf{x}}_{t+j\Delta t}^i, \mathbf{x}_{t+j\Delta t}^i)], \quad (6)$$

where  $\mathcal{L}_{pred}$  denotes the discrepancy error between the true state  $\mathbf{x}(t)$  and the predicted state  $\hat{\mathbf{x}}(t)$ . It has been well observed that ResNets work much similarly to a fixed step explicit *Euler* scheme [41, 33]. This connection has been further exploited to develop continuous normalizing flows [42].

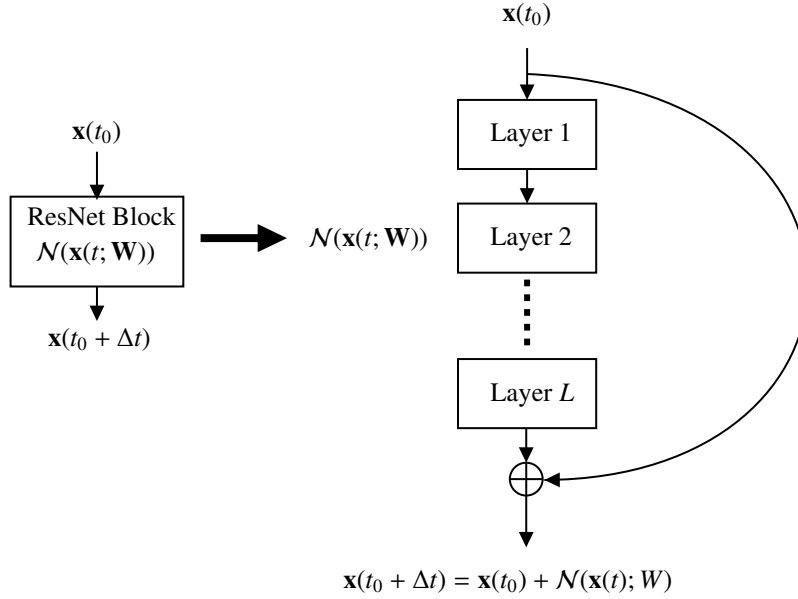


Figure 1: Residual neural network architecture

However, when dealing with systems exhibiting multiscale phenomena, a single discrete flow map operator  $\mathcal{N}()$  may not provide an accurate estimation across various time scales. As shown in [36], an NNTS model trained on coarse time steps fails to capture fine-scale information, while the prediction accuracy of the one trained on finer steps reduces rapidly due to the autoregression-based estimation process. This issue is addressed by using a combination of neural network models trained at different timescales, which can effectively capture both coarse and fine-scale behaviors. However, this approach requires extensive offline computational costs for training and cross-validating the model combinations, especially when dealing with large datasets. To overcome this drawback in the multiscale HiTS scheme, we propose the L-HiTS framework. This data-driven scheme remains computationally inexpensive while maintaining prediction accuracy at par with the multiscale HiTS scheme. This can have practical applications for systems that involve large datasets, such as PDEs. In the following, we describe the general methodology and the algorithm for the L-HiTS method.

### 3. Latent Hierarchical Time-Stepping (L-HiTS) scheme for multiscale PDEs

In order to accurately and efficiently predict dynamics, we need to complete two machine learning tasks. Firstly, we need to find a coordinate transformation that can represent the original multiscale dynamics onto a smaller subspace, using only a few latent variables. To achieve this, we use deep AE networks. Secondly, we need to discover the discrete-time flow maps for predictions within the latent space. This is done by using the multiscale HiTS scheme on the latent variables. Both tasks are described in more detail below.

#### 3.1. Discovery of coordinates using deep autoencoders

Autoencoders are a special class of neural networks that learn to compress the input data into a lower-dimensional representation and then reconstruct the original data from the learned representation. In this study, we incorporate deep AE models to learn a mapping  $\mathbf{f} : \mathbf{x}(t) \rightarrow \hat{\mathbf{x}}(t)$  from the input state vector  $\mathbf{x}(t)$  to its predicted output  $\hat{\mathbf{x}}(t)$  such that  $\hat{\mathbf{x}}(t) \approx \mathbf{x}(t)$ , where  $\mathbf{f} : \mathbb{R}^n \rightarrow \mathbb{R}^n$ . We use the *encoder* function of the autoencoder as a *restricting* operator that takes the input state measurements  $\mathbf{x}(t)$  from the dynamical system of dimension  $n$  and map it to a latent state vector  $\mathbf{z}(t) \in \mathbb{R}^z$  ( $z \ll n$ ) given as:

$$\mathbf{z}(t) = \mathbf{f}_E(\mathbf{x}(t); \mathbf{W}_E), \quad (7)$$

where  $\mathbf{f}_E(\cdot)$  is the nonlinear function learned by the encoder, and  $\mathbf{W}_E$  are the weights of the encoder network. The latent vector  $\mathbf{z}(t)$  is then passed through a *decoder* function that acts as a *lifting* operator, i.e., the decoder maps the latent vector  $\mathbf{z}(t)$  back to the high-dimensional reconstructed state vector  $\hat{\mathbf{x}}(t)$  given as:

$$\hat{\mathbf{x}}(t) = \mathbf{f}_D(\mathbf{z}(t); \mathbf{W}_D), \quad (8)$$

where  $\mathbf{f}_D(\mathbf{z}(t); \mathbf{W}_D)$  is the nonlinear function learned by the decoder network, and  $\mathbf{W}_D$  represents its weights. Thus, an AE network combines the restricting and lifting mechanisms to produce the reconstructed state  $\hat{\mathbf{x}}$  given as:

$$\hat{\mathbf{x}}(t) = \mathbf{f}_D(\mathbf{f}_E(\mathbf{x}(t); \mathbf{W}_E); \mathbf{W}_D). \quad (9)$$

The reconstructed state is obtained by finding the optimal weight matrix  $\mathbf{W} = \mathbf{W}_E, \mathbf{W}_D$  that minimizes the *reconstruction loss function*  $\mathbf{W}_{recon}^*$ , given as:

$$\mathbf{W}_{recon}^* = \arg \min_{\mathbf{W}} \frac{1}{N} \sum_{i=1}^N [\mathcal{L}_{recon}(\hat{\mathbf{x}}(t_i), \mathbf{x}(t_i))], \quad (10)$$

where  $\mathcal{L}_{recon}$  denotes the discrepancy error between  $\mathbf{x}(t)$  and  $\hat{\mathbf{x}}(t)$ . The condition  $z \ll n$  serves as a regularization term that prevents the AE model from learning an identity function. The schematic diagram of an AE is shown in Figure 2.

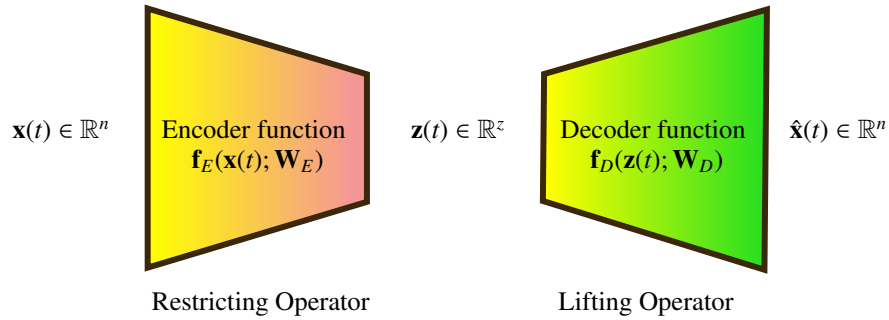


Figure 2: Schematic diagram of an autoencoder. The high dimensional input state  $\mathbf{x}(t)$  is restricted using an encoder function  $\mathbf{f}_E$  to obtain latent vector  $\mathbf{z}(t)$ , which is then passed through the lifting mechanism of the decoder function  $\mathbf{f}_D$  to obtain reconstructed state vector  $\hat{\mathbf{x}}(t)$ .

The use of an autoencoder model to identify the coarse-grained dynamics has several practical advantages. Firstly, the neural network-based design of the model enables it to be scaled up to a large size, which can be difficult with linear embedding-based techniques [44]. Secondly, the AE model describes both the encoding and decoding transformations employed during the process. This can be used within the EFF framework for multiscale applications, as demonstrated in a recent study [30].

### 3.2. Discovery of multiscale flow maps using deep residual neural networks

Once the latent coordinates are obtained using a deep AE model, we proceed to discover the flow-map representations of the latent variables. We accomplish this by using the multiscale HiTS scheme (described in [36]) within the latent space. The multiscale HiTS scheme involves learning different flow-map representations across various temporal scales. This is done using a hierarchy of deep neural network time steppers. The scheme uses deep ResNet models as building blocks to learn different flow-maps that advance the system dynamics forward in time. Given the data collected from the system at a unit time-step  $\Delta t$  sub-sampled uniformly at different multiples of  $\Delta t$ , i.e.,  $\Delta t_m = 2^{m-d} \Delta t$  ( $d = 1, 2, \dots, m$ ), the multiscale HiTS scheme learns multiple flow maps  $\mathcal{N}_m(\cdot; \Delta t_m)$  that captures the system dynamics across timescales. The NNTS model with a large temporal gap captures the slow scale behavior, while the NNTS model with the smallest temporal gap captures the fast scale features of the system.

After learning the different flow map representations, the scheme couples the output of different NNTS models  $\text{RN}_1, \text{RN}_2, \dots, \text{RN}_m$  using an iterative vectorized fashion (see Algorithm 1 of [36]). The process involves using the

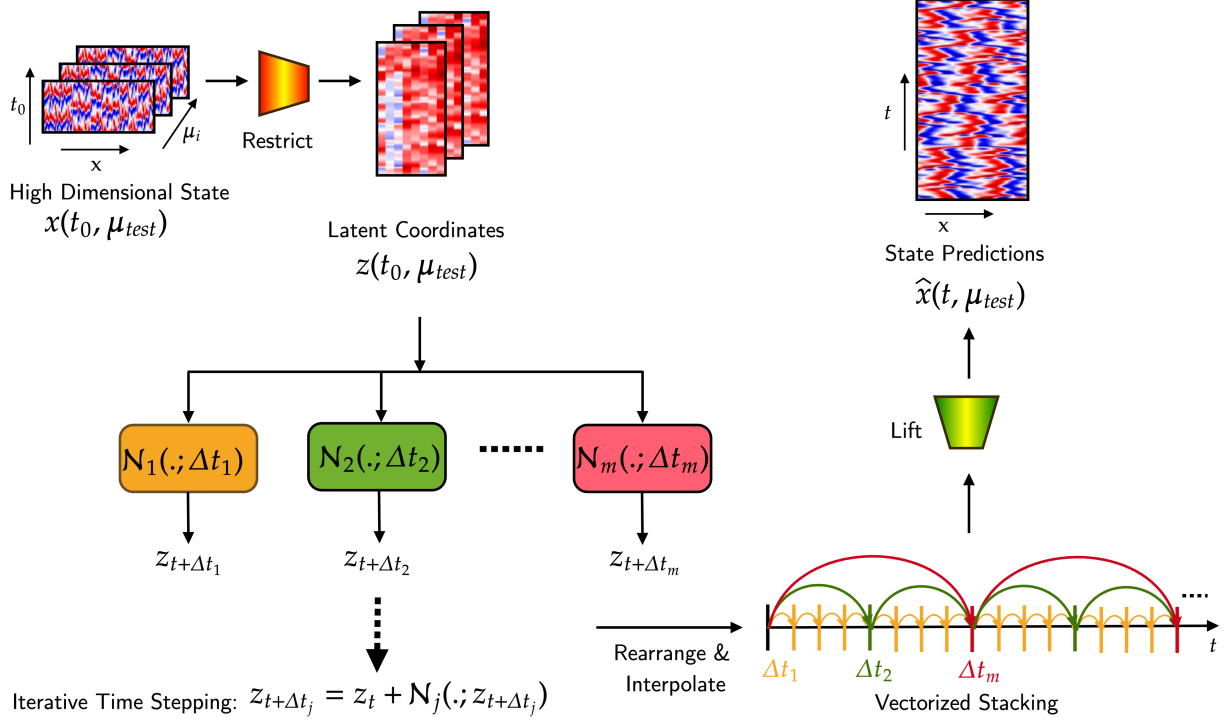


Figure 3: Block diagram of the proposed L-HiTS method

NNTS model with the largest temporal gap first to make predictions. These predictions are then passed on to the next level NNTS model, and its outputs are stacked together with the previous one. This process continues until the smallest NNTS model is used. After rearranging the predictions, an interpolation scheme is used to determine the predictions between time steps. By doing this, the error propagation from individual NNTS models can be eliminated. Before coupling the individual NNTS models for multiscale applications, the HiTS scheme uses a cross-validation step to filter out the best possible combination of NNTS models. This step is essential as the accuracy of individual NNTS models may vary, which could lead to inaccurate predictions after coupling. However, this process can be computationally expensive, especially for large-scale systems where the sampled data is extensive. To address this shortcoming, an adaptive hierarchical time stepping (AHITS) method has been proposed [45] which adapts the time-step, i.e., the choice of NNTS model during the simulation, based on system dynamics.

### 3.3. Combining deep AEs and multiscale HiTS scheme for multiscale predictions

The proposed L-HiTS scheme combines the use of coordinates and flow maps for multiscale predictions within the latent space. We begin by collecting  $p$  trajectories of the dynamical system state  $\mathbf{x}(t)$  at  $t_f$  instances of the unit time step  $\Delta t$  and stack inside a matrix  $\mathbf{X}$  given as:

$$\mathbf{X}^i = [\mathbf{x}^i(t_0) \quad \mathbf{x}^i(t_0 + \Delta t) \quad \dots \quad \mathbf{x}^i(t_0 + t_f \Delta t)], \quad (11)$$

where  $i \in 1, \dots, p$ . The data is divided into training, validation, and testing datasets. The training data is compressed using the restricting action of the encoder function within the AE model to obtain the latent variables  $\mathbf{z}(t)$ . These latent variables are then fed to individual NNTS models  $\text{RN}_1$  to  $\text{RN}_m$  as per the respective step sizes. For instance, the  $\text{RN}_1$  model uses the first  $t_f - 1$  entries of  $\mathbf{z}(t)$ , i.e.,  $[\mathbf{z}^i(t_0), \dots, \mathbf{z}^i(t_0 + (t_f - 1)\Delta t)]$  as the input and one  $\Delta t$  ahead entries, i.e.,  $[\mathbf{z}^i(t_0 + \Delta t), \dots, \mathbf{z}^i(t_0 + t_f \Delta t)]$  as the output. By doing so, each NNTS model learns its respective flow map  $\mathcal{N}_m(\mathbf{z}(t); \Delta t_m)$  to obtain the future predictions of the latent variables from a given initial condition  $t_0$ , which is given

as:

$$\mathbf{z}(t_0 + \Delta t_m) = \mathbf{z}(t_0) + \mathcal{N}_m(\mathbf{z}(t); \Delta t_m). \quad (12)$$

After the individual responses are obtained, we use the validation dataset to cross-validate the NNTS models for coupling, as described above. Using iterative vectorized computations from [36], we obtain the future predictions in the latent space. The solution thus obtained is finally lifted using the decoder function within the AE model. Figure 3 provides a summary of the L-HiTS scheme. We can use the L-HiTS scheme to obtain future state predictions for any testing initial condition  $\mathbf{x}_0$ . For an unknown system parameter  $\mu_{test}$ , we pass the testing initial condition through the encoder block to obtain the initial condition in the latent space  $\mathbf{z}_0$ . We then utilize the multiscale HiTS framework to initialize the iterative one-step ahead predictions within the latent space for a given time span  $[t_0, T]$ . The predictions within the latent space are then obtained directly using the multiscale HiTS scheme. Finally, we pass the solutions obtained through the decoder function to reconstruct the original state variable  $\hat{\mathbf{x}}(t)$ . The pseudocode for the L-HiTS procedure can be found in Algorithm 1. In the next section, we will demonstrate the application of the L-HiTS scheme using numerical simulations.

---

**Algorithm 1** : L-HiTS Algorithm

---

**Input:** ResNet models:  $RN_1, \dots, RN_m$ , initial condition  $\mathbf{x}_0$

**Output:** Reconstructed states  $\hat{\mathbf{x}}$ .

```

1: sort(RN models)                                ◦ in descending order as per trained step sizes.
2:  $\mathbf{Z} = \text{list}\{\}$ 
3:  $\mathbf{z} = f_E(\mathbf{x}_0)$                                 ◦ Encode the initial condition
4: append( $\mathbf{Z}, \mathbf{z}$ )                                ◦ Append the encoded initial condition to  $\mathbf{z}$ 
5: for  $k=1, 2, \dots, m$  do
6:    $Q_k :=$  number of forward steps.
7:    $\mathbf{z}_c = \text{stack}(\mathbf{z})$                             ◦ stack states together
8:    $\mathbf{z}_n = RN_k.\text{forward}(\mathbf{z}_c, \mathbf{z})$             ◦ use Algorithm 1 of [36] to obtain  $\mathbf{z}_n$ 
9:   append( $\mathbf{z}_n, \mathbf{z}$ )                                ◦ update the predicted states
10: end for
11: rearrange( $\mathbf{z}$ )
12: Interpolate( $\mathbf{z}$ )
13:  $\hat{\mathbf{X}} = f_D(\mathbf{z})$                                 ◦ Decode the reduced states
14: return( $\hat{\mathbf{x}}$ )                                    ◦ Return the reconstructed states

```

---

## 4. Simulation results

To demonstrate the application of the L-HiTS scheme, we consider two benchmark PDEs. The FitzHugh-Nagumo (FHN) model [46, 47] and the 1D Kuramoto-Sivashinsky (KS) equation [48, 49]. To facilitate comparison with the multiscale HiTS method, all the model parameters and data structures are kept the same. To test the accuracy of the methods, we use the mean squared error (MSE) as a metric for comparison. All the simulations are performed using the open source Python API for PyTorch framework running on hp workstation Z1 with 11<sup>th</sup> Gen Intel(R) Core (TM) i7-11700 @2.5GHz CPU. However, the code that we accompany with this manuscript is written to take advantage of faster computations via GPU if available.

### 4.1. The FitzHugh-Nagumo model

The FHN model is a simplified 2D version of the *Hodgkin-Huxley* model that describes the activation and deactivation dynamics of a spiking neuron. The membrane potential is described by a single variable,  $\mathbf{u}(\mathbf{x}, t)$ , known as the *inhibitor*, and the activation/deactivation dynamics of the voltage-gated ion channels are represented by another variable,  $\mathbf{v}(\mathbf{x}, t)$ , known as the *activator*. The governing equation consists of two coupled nonlinear differential equations

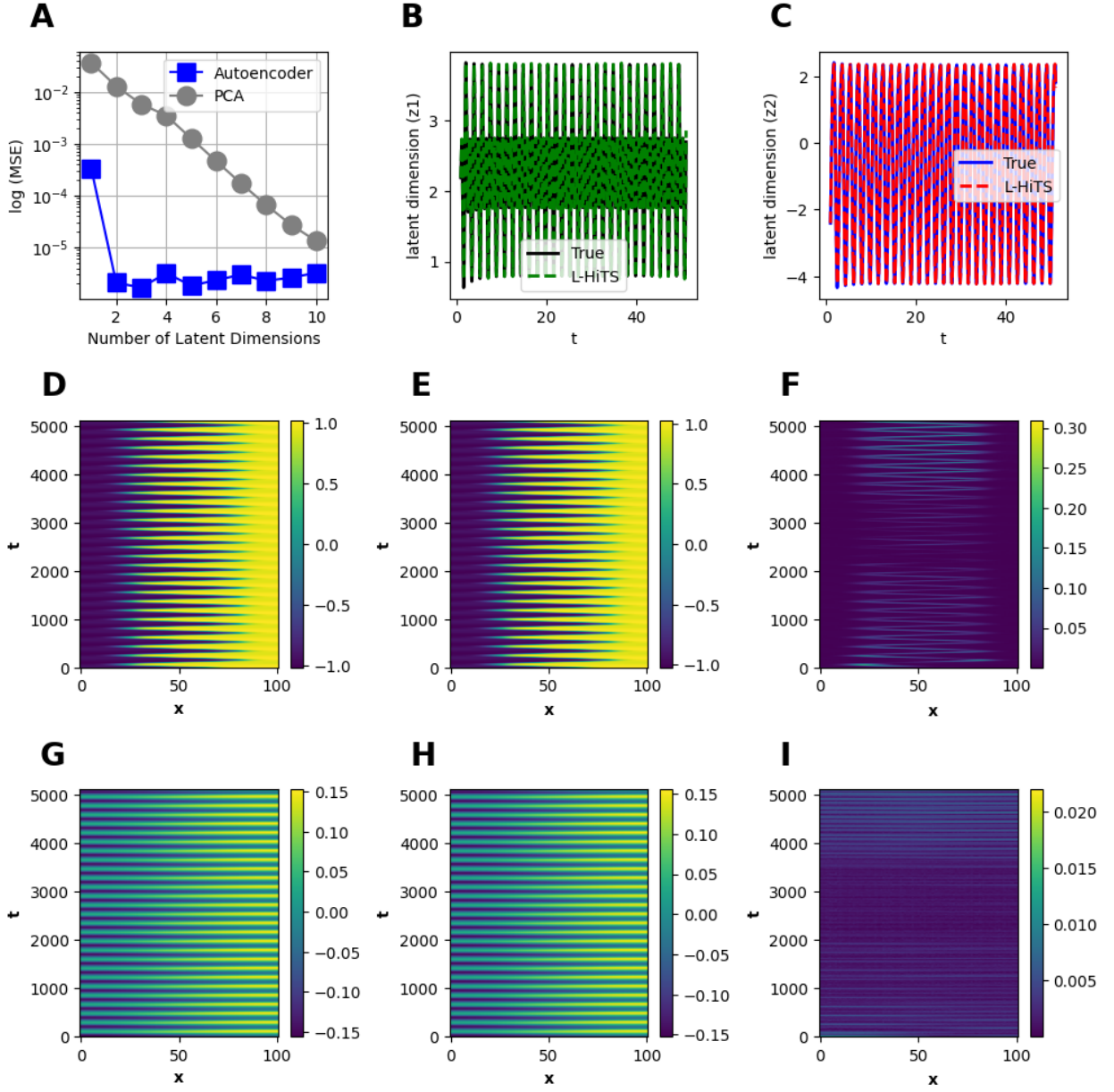


Figure 4: Results for the FHN model: (Plot A:) plot of the MSEs for autoencoder and PCA for testing dataset against varying latent dimensions (Plot B-C:) evolution of latent variables  $z_1(t)$  and  $z_2(t)$  obtained from AE and L-HiTS scheme, (Plot D:) true state  $\mathbf{u}(\mathbf{x}, t)$ , (Plot E:) predicted state  $\hat{\mathbf{u}}(\mathbf{x}, t)$  from the L-HiTS scheme, (Plot F:) MSE between  $\hat{\mathbf{u}}(\mathbf{x}, t)$  and  $\hat{\mathbf{u}}(\mathbf{x}, t)$ , (Plot G:) true state  $\mathbf{v}(\mathbf{x}, t)$ , (Plot H:) predicted state  $\hat{\mathbf{v}}(\mathbf{x}, t)$  from the L-HiTS scheme, (Plot I:) MSE between  $\hat{\mathbf{v}}(\mathbf{x}, t)$  and  $\hat{\mathbf{v}}(\mathbf{x}, t)$ .

that describe the time evolution of  $\mathbf{u}(\mathbf{x}, t)$  and  $\mathbf{v}(\mathbf{x}, t)$  given as;

$$\begin{aligned}
 \epsilon \frac{\partial \mathbf{u}}{\partial t}(\mathbf{x}, t) &= \epsilon^2 \frac{\partial \mathbf{u}^2}{\partial \mathbf{x}^2}(\mathbf{x}, t) + \mathbf{f}(\mathbf{u}(\mathbf{x}, t) - \mathbf{v}(\mathbf{x}, t) + 0.05, \\
 \frac{\partial \mathbf{v}}{\partial t}(\mathbf{x}, t) &= 0.5\mathbf{u}(\mathbf{x}, t) - 2\mathbf{v}(\mathbf{x}, t) + 0.05,
 \end{aligned}
 \tag{13}$$



where  $\mathbf{f}(\mathbf{u}) = \mathbf{u}(\mathbf{u} - 0.1)(1 - \mathbf{u})$ . The model exhibits multiscale behavior with activator  $\mathbf{u}(\mathbf{x}, t)$  showing fast dynamics, whereas inhibitor  $\mathbf{v}(\mathbf{x}, t)$  has slower dynamics. The difference is controlled by the parameter  $\epsilon = 0.015$ . The initial and boundary conditions are taken from [50]. Using Lattice Boltzmann (LB) method [51], (13) is discretized using  $n = 202$ , grid points in space and  $T = 5120$  grid points in time. We utilize the LB method to collect data from six different initial conditions in order to derive the true solution of the system similar to [50, 30]. We consider four initial conditions for training purposes, one for validation, and a different initial condition is used for testing the accuracy of the L-HiTS method. To identify the latent space, we use the principle component analysis (PCA) method and AE by comparing the MSE of reconstruction on the test data. Figure 4, plot A shows the comparison in terms of MSE against the number of latent dimensions  $z$ . As can be seen, AE outperforms PCA by identifying a nonlinear subspace that effectively reduces the dimensionality to  $z = 2$ , and then the latent dimension size remains constant. This indicates that the underlying solution space has an intrinsic dimensionality of order two. The various network parameters for this case are enlisted in Appendix A, Table 5. The plots B and C of the same figure show the evolution of the two latent variables obtained from the AE model and the corresponding predictions from the L-HiTS scheme. As can be seen, the true and predicted dynamics are graphically indistinguishable. Numerically, the accuracy of the L-HiTS scheme for varying latent dimensions for both latent and reconstructed variables can be seen in Table 1. The results show that the MSE plateaus after the latent dimension of  $z = 2$ , which is also reflected in the MSEs of the output predictions and we use this for initialization of the L-HiTS scheme. The plots D-I of Figure 4 show the corresponding space-time plots for both the variables  $\mathbf{u}(\mathbf{x}, t)$  and  $\mathbf{v}(\mathbf{x}, t)$  which shows a good agreement between the true and the predicted solution. The computational costs of the L-HiTS method are shown in Table 2, where the efficiency of the L-HiTS scheme against the multiscale HiTS scheme can be observed both during the training and prediction stages.

#### 4.2. The 1D Kuramoto-Sivashinsky equation

To test the proposed L-HiTS scheme on a more challenging system, we take the 1D KS equation that exhibits spatiotemporal chaos and is used to describe various physical phenomena such as chemical reactions, turbulence, and flame fronts. The system dynamics are described by a fourth-order nonlinear PDE defined as:

$$\mathbf{u}_t = -\mathbf{u}\mathbf{u}_x - \frac{1}{2}\mathbf{u}_{xx} - \mathbf{u}_{xxx} \quad (14)$$

for  $x \in [-L/2, L/2]$  with  $n = 120$  grids points and a periodic boundary condition  $\mathbf{u}(0; t) = \mathbf{u}(L; t)$  and some given initial conditions. We simulate the KS equation using a fourth-order stiff time-stepping (ETDRK4) method [52] with  $t \in [0, 5121]$  with a step size of  $\Delta t = 0.05$ . We consider the case of  $L = 22$  as considered in [53, 30] for which the system exhibits a structurally stable chaotic attractor, i.e., an inertial manifold in which the long-term behavior of the system lies. For the training phase of the L-HiTS method, we take  $\mu_{train} = 10$  random, periodic initial conditions,  $\mu_{val} = 5$  initial conditions for the validation, and  $\mu_{test} = 5$  random initial conditions for testing purposes. For the identification of the latent space, we compare the PCA and AE models in terms of reconstruction MSE in the test data as a function of latent dimension  $z$ , graphically shown in plot A of Figure 5 and numerically enlisted in Table 1. We observe that the MSE plateaus after  $z = 8$ , in agreement with [53, 30]. Thus, we chose a latent dimension of  $z = 8$  for the L-HiTS framework. We also compared the different latent variables obtained by the L-HiTS scheme against the testing data encoded within the latent space. These are shown in plots B-I of Figure 5, and the corresponding hyperparameters, including the network architectures of the AE and different ResNet models, are enlisted in Appendix A, Table 6. As observed, the L-HiTS method correctly estimates the evolution of the latent variables in time.

To predict the chaotic dynamics within the latent space, we use  $m = 11$  NNTS models trained on the outputs from the encoder. After coupling the individual NNTS models, the output is reconstructed using the decoder function within the AE model. The original and reconstructed space-time plots are shown in plots J and K of Figure 5 respectively, with the error in plot L. The results show that the L-HiTS scheme satisfactorily reconstructs the true chaotic dynamics of the KS equation. Furthermore, the computational costs of the L-HiTS scheme against the multiscale HiTS scheme are presented in Table 2. As expected, the L-HiTS method yields almost one order of magnitude saving than the multiscale HiTS scheme in predicting dynamics and a lesser training time while maintaining the same accuracy. This substantiates our observation that learning multiple flow maps of the system within the latent space yields an efficient state prediction in the original solution space.

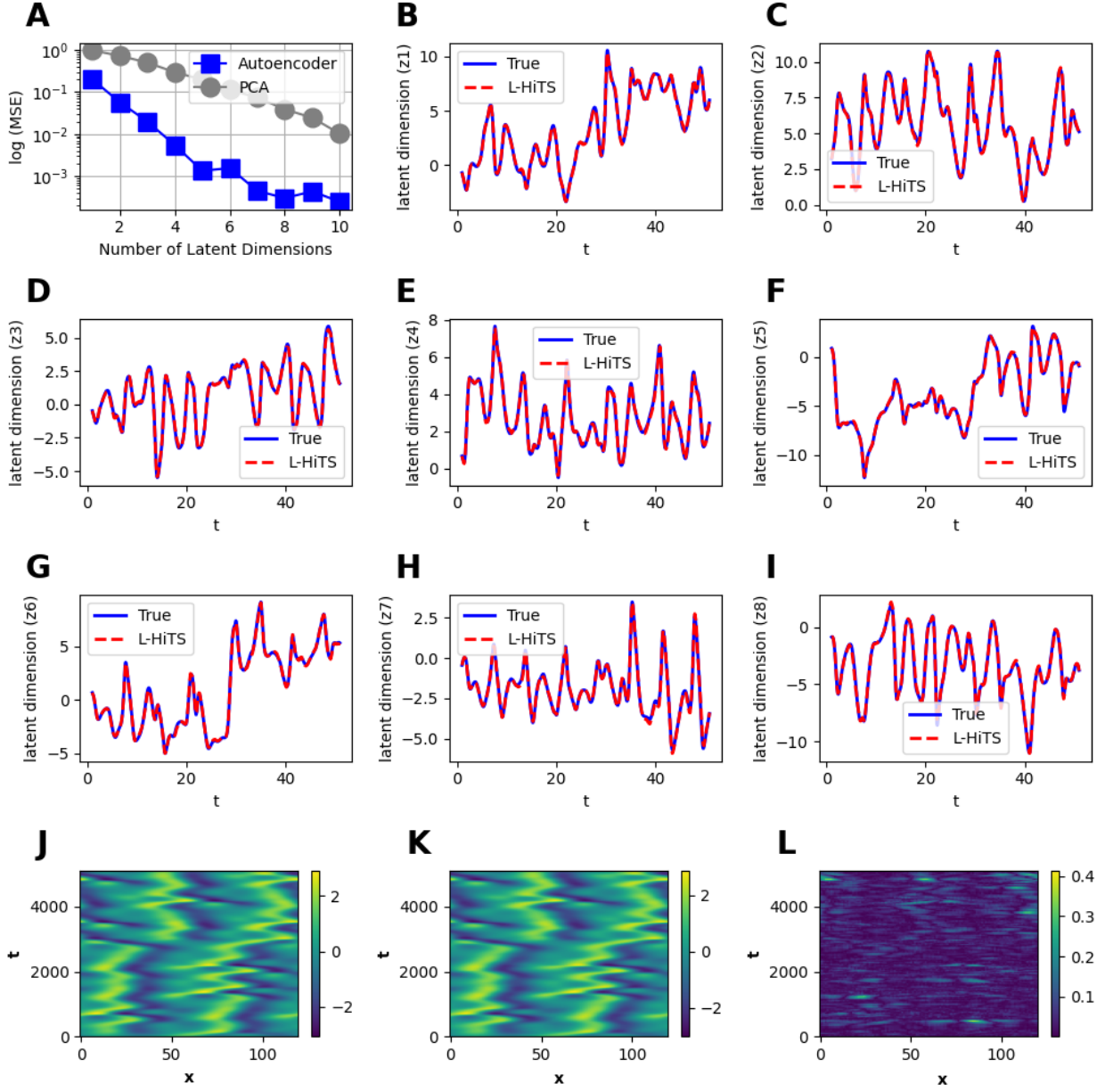


Figure 5: Results for the 1D KS equation: (Plot A:) plot of MSEs for autoencoder and PCA for testing dataset against varying latent dimensions, (Plot B-I:) evolution of the latent variables  $z_1(t), \dots, z_8(t)$  obtained from the AE model and L-HiTS scheme, (Plot J:) true solution of the state  $u(x, t)$ , (Plot K:) predicted state  $\hat{u}(x, t)$  from the L-HiTS scheme, (Plot L:) MSE between  $u(x, t)$  and  $\hat{u}(x, t)$

Table 1: MSEs for the FHN model and KS equation obtained using the L-HiTS method for varying dimensions of latent space

Latent dimension	FHN model		KS equation	
	Latent space (MSE)	Reconstruction (MSE)	Latent space (MSE)	Reconstruction (MSE)
1	$2.34 \times 10^0$	$2.44 \times 10^{-1}$	$6.79 \times 10^1$	$2.26 \times 10^0$
2	$1.47 \times 10^{-3}$	$1.37 \times 10^{-4}$	$5.01 \times 10^1$	$2.41 \times 10^0$
4	$2.42 \times 10^{-2}$	$2.20 \times 10^{-3}$	$4.73 \times 10^1$	$1.30 \times 10^0$
6	$2.79 \times 10^{-2}$	$3.60 \times 10^{-3}$	$1.90 \times 10^{-2}$	$4.05 \times 10^{-3}$
8	$2.13 \times 10^{-3}$	$2.88 \times 10^{-4}$	$1.35 \times 10^{-3}$	$1.50 \times 10^{-3}$
10	$5.96 \times 10^{-3}$	$9.97 \times 10^{-4}$	$3.16 \times 10^{-3}$	$1.42 \times 10^{-3}$

Table 2: Comparison of accuracy and computational cost

Technique	FHN model			KS equation		
	Training time	Prediction time	$\ell_2$ -norm error	Training time	Prediction time	$\ell_2$ -norm error
Multiscale-HiTS [36]	1767s	8.08s	$2 \times 10^{-4}$	1982s	20.88s	$4 \times 10^{-3}$
L-HiTS (proposed)	1248s	3.52s	$2 \times 10^{-4}$	1624s	2.86s	$4 \times 10^{-3}$

## 5. Discussions and conclusion

In this section, we provide some additional comments regarding the sensitivity of the L-HiTS scheme for different network choices, followed by some concluding remarks toward the end.

### 5.1. Effect of different latent dimensions

To evaluate the sensitivity of the L-HiTS method for different latent sizes, we calculate the mean square errors for both the latent and reconstruction states, as shown in Table 1. Additionally, we plot the MSEs for different time steps during the forecasting stage, as presented in Figure 6. Our results indicate that for both test cases, increasing the latent dimension of the autoencoder model reduces the mean square error. This means that a larger dimension of the latent space implies that there are more basis functions to express the encoded information about the system, which is in agreement with [23]. However, we found that the MSE saturates beyond  $z = 2$  for the FHN system and  $z = 8$  for the case of the KS equation, indicating that no further improvement in forecasting accuracy can be achieved.

In the context of machine learning, the relationship between accuracy in latent space and reconstruction accuracy is complex and can vary depending on the model architecture and the specific application. In general, there isn't a direct correlation where higher accuracy in latent space straightforwardly results in higher reconstruction accuracy. However, our findings are aligned with [23], wherein authors have established a similar relationship between the latent dimensions and reconstruction accuracy. The authors therein report a reduced  $\mathcal{L}^2$  reconstruction error as the latent dimension of the autoencoder model is increased. Besides, there are contexts and specific methods where improvements in latent representation can enhance reconstruction quality, such as the use of sparse and denoising autoencoders [54, 53], variational autoencoders [55], and deep embedding clustering[56]. While our framework currently incorporates a basic version of the autoencoder, it can easily incorporate these variations of autoencoders with only minor adjustments. This will ensure that the relationship between latent space and reconstruction will remain consistent.

### 5.2. Effect of individual and multiple models within the latest space

To check the effect of individual NNTS models on the quality of output prediction and computational costs, we use each individual NNTS model within the latent space and compare that with the coupling framework used in the L-HiTS scheme. The results are shown in Tables 3 and 4. As observed from the results, models with small time

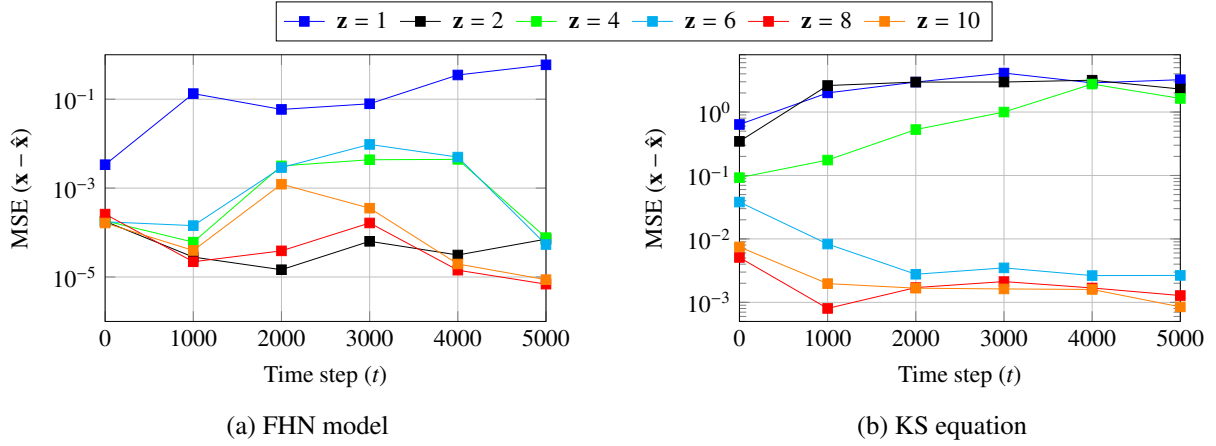


Figure 6: Sensitivity analysis: mean square error of state predictions at different time-steps for varying latent space dimension  $z$ .

Table 3: FHN model: comparison of MSE and CPU times across various NNTS models at a latent dimension of  $z = 2$

Model	MSE ( $x - \hat{x}$ )	CPU times (seconds)
RN <sub>1</sub>	$3.73 \times 10^{-1}$	1.22
RN <sub>2</sub>	$3.55 \times 10^{-1}$	0.66
RN <sub>4</sub>	$2.36 \times 10^{-1}$	0.29
RN <sub>8</sub>	$3.52 \times 10^{-3}$	0.14
RN <sub>16</sub>	$2.26 \times 10^{-3}$	0.07
RN <sub>32</sub>	$8.07 \times 10^{-3}$	0.04
RN <sub>64</sub>	$6.04 \times 10^{-2}$	0.01
RN <sub>128</sub>	$2.58 \times 10^{-1}$	0.01
RN <sub>256</sub>	$2.92 \times 10^{-1}$	0.006
RN <sub>512</sub>	$3.14 \times 10^{-1}$	0.003
RN <sub>1024</sub>	$2.85 \times 10^{-1}$	0.002
<b>L-HiTS</b>	$1.37 \times 10^{-4}$	3.52

steps yield accurate short-term predictions; however, the error quickly accumulates due to autoregressive predictions, making the overall reconstruction quite poor. In contrast, networks with larger temporal gaps yield better long-term predictions but fail to capture information between steps. Thus, models with intermediate time steps, such as RN<sub>16</sub> in the case of the FHN model and RN<sub>64</sub> in the case of the KS equation, balance out the two factors, resulting in a better MSE that the proposed method effectively captures, thus outperforming any individual NNTS model. The computation time, on the other hand, accelerates as the step size grows, and the proposed method provides a good trade-off between accuracy and efficiency.

### 5.3. Concluding remarks

In this study, we propose a novel framework that enhances the computational efficiency of multiscale PDEs. Our strategy is based on the idea of learning coordinates and flow maps using deep neural networks that enable rapid and accurate predictions of future states. The proposed L-HiTS method uses deep autoencoder networks to learn suitable latent coordinates that represent the dynamics on a low-dimensional basis. Then, we make use of the existing multiscale HiTS method within the discovered latent space to obtain multiple flow maps that march the latent variables in time. The predictions are then lifted to the original space using the decoder function of the AE model. The method outperforms any individual neural network time stepper model in terms of accuracy and the original multiscale HiTS method in terms of computational costs. We demonstrate the application of the proposed scheme on two large-scale PDEs with multiscale physics.

Table 4: KS equation: comparison of MSE and CPU times across various NNTS models at a latent dimension of  $z = 8$ .

Model	MSE ( $x - \hat{x}$ )	CPU times (seconds)
RN <sub>1</sub>	1.97	0.79
RN <sub>2</sub>	2.77	0.37
RN <sub>4</sub>	2.68	0.19
RN <sub>8</sub>	2.47	0.09
RN <sub>16</sub>	1.67	0.04
RN <sub>32</sub>	1.10	0.02
RN <sub>64</sub>	$1.09 \times 10^{-2}$	0.01
RN <sub>128</sub>	$8.74 \times 10^{-2}$	0.009
RN <sub>256</sub>	$4.04 \times 10^{-1}$	0.0055
RN <sub>512</sub>	$9.69 \times 10^{-1}$	0.0037
RN <sub>1024</sub>	1.29	0.0029
<b>L-HiTS</b>	$1.50 \times 10^{-3}$	2.86

Although the proposed method works well, there are some potential drawbacks that can be taken up in a future study. Firstly, the proposed method assumes full-state observations, meaning that all the time-dependent states are available across a diverse range of operating conditions. However, in many practical scenarios, only partial measurements are available. To address this issue, a time delay embedded of the partial measurements can be used ( see, e.g., [57, 58]) within the L-HiTS framework to make it more practical. Secondly, the L-HiTS framework uses fixed step size-based predictions of the latent states within the individual ResNet models. This can be computationally expensive if some of the latent variables evolve faster than the rest. To address this issue, an adaptive time-step-based strategy can be used within the latent space, where the time step can be adjusted based on the evolving dynamics.

#### Credit authorship contribution statement

**Asif Hamid:** Software, Methodology, Data-curation, Validation, Writing- original draft,

**Danish Rafiq:** Conceptualization, Methodology, Funding acquisition, Investigation, Writing- Reviewing and Editing,

**Shahkar A. Nahvi:** Supervision, Reviewing,

**Mohammad A. Bazaz:** Supervision, Reviewing

#### Declaration of competing interest

The authors declare no potential financial or non-financial competing interests

#### Acknowledgments

Author I would like to acknowledge the Doctoral fellowship from the Islamic University of Science and Technology, Kashmir, India, via Grant No. IUST0119013135, and Author II, acknowledges the financial assistance from the Science and Engineering Research Board (SERB), a statutory body of the Department of Science and Technology (DST), Government of India, via Grant No. PDF/2022/002081.

#### Code availability

The source code is available at <https://github.com/erasifhamid/L-HiTS>

## References

- [1] J. H. Mathews, Numerical methods for mathematics, science and engineering, Vol. 10, Prentice-Hall International, 1992.
- [2] J. Bezanson, A. Edelman, S. Karpinski, V. B. Shah, Julia: A fresh approach to numerical computing, *SIAM review* 59 (1) (2017) 65–98.
- [3] S. D. Conte, C. De Boor, Elementary numerical analysis: an algorithmic approach, SIAM, 2017.
- [4] J. W. Thomas, Numerical partial differential equations: finite difference methods, Vol. 22, Springer Science & Business Media, 2013.
- [5] E. Weinan, Principles of multiscale modeling, Vol. 1, Cambridge University Press, 2011.
- [6] O. Ghattas, K. Willcox, Learning physics-based models from data: perspectives from inverse problems and model reduction, *Acta Numerica* 30 (2021) 445–554.
- [7] W. Gong, Q. Duan, J. Li, C. Wang, Z. Di, Y. Dai, A. Ye, C. Miao, Multi-objective parameter optimization of common land model using adaptive surrogate modeling, *Hydrology and Earth System Sciences* 19 (5) (2015) 2409–2425.
- [8] E. A. Groen, R. Heijungs, E. A. Bokkers, I. J. De Boer, Methods for uncertainty propagation in life cycle assessment, *Environmental Modelling & Software* 62 (2014) 316–325.
- [9] M. Taufer, E. Deelman, R. F. da Silva, T. Estrada, M. Hall, M. Livny, A roadmap to robust science for high-throughput applications: The developers’ perspective, in: 2021 IEEE International Conference on Cluster Computing (CLUSTER), IEEE, 2021, pp. 807–808.
- [10] G. Novati, H. L. de Laroussilhe, P. Koumoutsakos, Automating turbulence modelling by multi-agent reinforcement learning, *Nature Machine Intelligence* 3 (1) (2021) 87–96.
- [11] S. Verma, G. Novati, P. Koumoutsakos, Efficient collective swimming by harnessing vortices through deep reinforcement learning, *Proceedings of the National Academy of Sciences* 115 (23) (2018) 5849–5854.
- [12] J. J. Bramburger, D. Dylewsky, J. N. Kutz, Sparse identification of slow timescale dynamics, *Physical Review E* 102 (2) (2020) 022204.
- [13] Kevrekidis, et al., Equation-free, coarse-grained multiscale computation: enabling microscopic simulators to perform system-level analysis, *Commun. Math. Sci* 1 (4) (2003) 715–762.
- [14] I. G. Kevrekidis, C. W. Gear, G. Hummer, Equation-free: The computer-aided analysis of complex multiscale systems, *AIChE Journal* 50 (7) (2004) 1346–1355.
- [15] E. Weinan, B. Engquist, The heterogenous multiscale methods, *Communications in Mathematical Sciences* 1 (1) (2003) 87–132.
- [16] M. Tao, H. Owghadi, J. E. Marsden, Nonintrusive and structure preserving multiscale integration of stiff odes, sdes, and hamiltonian systems with hidden slow dynamics via flow averaging, *Multiscale Modeling & Simulation* 8 (4) (2010) 1269–1324.
- [17] R. Ganesan, T. K. Das, V. Venkataraman, Wavelet-based multiscale statistical process monitoring: A literature review, *IIE transactions* 36 (9) (2004) 787–806.
- [18] J. N. Kutz, X. Fu, S. L. Brunton, Multiresolution dynamic mode decomposition, *SIAM Journal on Applied Dynamical Systems* 15 (2) (2016) 713–735.
- [19] S. G. Mallat, A theory for multiresolution signal decomposition: the wavelet representation, *IEEE transactions on pattern analysis and machine intelligence* 11 (7) (1989) 674–693.
- [20] R. Vinuesa, S. L. Brunton, Enhancing computational fluid dynamics with machine learning, *Nature Computational Science* 2 (6) (2022) 358–366.
- [21] Z. Zhang, R. Rai, S. Chowdhury, D. Doermann, Midphynet: Memorized infusion of decomposed physics in neural networks to model dynamic systems, *Neurocomputing* 428 (2021) 116–129.
- [22] N. A. K. Doan, W. Polifke, L. Magri, Physics-informed echo state networks, *Journal of Computational Science* 47 (2020) 101237.
- [23] V. Oommen, K. Shukla, S. Goswami, R. Dingreville, G. E. Karniadakis, Learning two-phase microstructure evolution using neural operators and autoencoder architectures, *npj Computational Materials* 8 (1) (2022) 190.
- [24] T. Gracious, S. Gupta, A. Kanthali, R. M. Castro, A. Dukkipati, Neural latent space model for dynamic networks and temporal knowledge graphs, in: Proceedings of the AAAI Conference on Artificial Intelligence, Vol. 35, 2021, pp. 4054–4062.
- [25] J. Fish, G. J. Wagner, S. Keten, Mesoscopic and multiscale modelling in materials, *Nature materials* 20 (6) (2021) 774–786.
- [26] M. Meier-Schellersheim, I. D. Fraser, F. Klauschen, Multiscale modeling for biologists, *Wiley Interdisciplinary Reviews: Systems Biology and Medicine* 1 (1) (2009) 4–14.
- [27] M. Garbey, M. Rahman, S. Berceci, A multiscale computational framework to understand vascular adaptation, *Journal of computational science* 8 (2015) 32–47.
- [28] C. Wehmeyer, F. Noé, Time-lagged autoencoders: Deep learning of slow collective variables for molecular kinetics, *The Journal of chemical physics* 148 (24) (2018) 241703.
- [29] P. R. Vlachas, J. Zavadlav, M. Praprotnik, P. Koumoutsakos, Accelerated simulations of molecular systems through learning of effective dynamics, *Journal of Chemical Theory and Computation* 18 (1) (2021) 538–549.
- [30] P. R. Vlachas, G. Arampatzis, C. Uhler, P. Koumoutsakos, Multiscale simulations of complex systems by learning their effective dynamics, *Nature Machine Intelligence* 4 (4) (2022) 359–366.
- [31] I. Kičić, P. R. Vlachas, G. Arampatzis, M. Chatzimanolakis, L. Guibas, P. Koumoutsakos, Adaptive learning of effective dynamics for online modeling of complex systems, *Computer Methods in Applied Mechanics and Engineering* 415 (2023) 116204.
- [32] J. J. Bramburger, J. N. Kutz, Poincaré maps for multiscale physics discovery and nonlinear floquet theory, *Physica D: Nonlinear Phenomena* 408 (2020) 132479.
- [33] T. Qin, K. Wu, D. Xiu, Data driven governing equations approximation using deep neural networks, *Journal of Computational Physics* 395 (2019) 620–635.
- [34] L. Ying, E. J. Candes, The phase flow method, *Journal of Computational Physics* 220 (1) (2006) 184–215.
- [35] S. Recanatani, M. Farrell, G. Lajoie, S. Deneve, M. Rigotti, E. Shea-Brown, Predictive learning as a network mechanism for extracting low-dimensional latent space representations, *Nature communications* 12 (1) (2021) 1417.
- [36] Y. Liu, J. N. Kutz, S. L. Brunton, Hierarchical deep learning of multiscale differential equation time-steppers, *Philosophical Transactions of the Royal Society A* 380 (2229) (2022) 20210200.
- [37] K. Atkinson, W. Han, D. E. Stewart, Numerical solution of ordinary differential equations, John Wiley & Sons, 2011.

- [38] J. C. Butcher, *The numerical analysis of ordinary differential equations: Runge-Kutta and general linear methods*, Wiley-Interscience, 1987.
- [39] J. Guckenheimer, P. Holmes, *Nonlinear oscillations, dynamical systems, and bifurcations of vector fields*, Vol. 42, Springer Science & Business Media, 2013.
- [40] S. Wiggins, S. Wiggins, M. Golubitsky, *Introduction to applied nonlinear dynamical systems and chaos*, Vol. 2, Springer, 2003.
- [41] B. Chang, L. Meng, E. Haber, F. Tung, D. Begert, Multi-level residual networks from dynamical systems view, *arXiv preprint arXiv:1710.10348* (2017).
- [42] R. T. Chen, Y. Rubanova, J. Bettencourt, D. K. Duvenaud, Neural ordinary differential equations, *Advances in neural information processing systems* 31 (2018).
- [43] K. He, X. Zhang, S. Ren, J. Sun, Deep residual learning for image recognition, in: *Proceedings of the IEEE conference on computer vision and pattern recognition*, 2016, pp. 770–778.
- [44] T. Simpson, N. Dervilis, E. Chatzi, Machine learning approach to model order reduction of nonlinear systems via autoencoder and lstm networks, *Journal of Engineering Mechanics* 147 (10) (2021) 04021061.
- [45] A. Hamid, D. Rafiq, S. A. Nahvi, M. A. Bazaz, Hierarchical deep learning-based adaptive time-stepping scheme for multiscale simulations, *arXiv preprint arXiv:2311.05961* (2023).
- [46] R. FitzHugh, Impulses and physiological states in theoretical models of nerve membrane, *Biophysical journal* 1 (6) (1961) 445–466.
- [47] T. Nakamura, K. Fukami, K. Hasegawa, Y. Nabaie, K. Fukagata, Convolutional neural network and long short-term memory based reduced order surrogate for minimal turbulent channel flow, *Physics of Fluids* 33 (2) (2021) 025116.
- [48] Y. Kuramoto, Diffusion-induced chaos in reaction systems, *Progress of Theoretical Physics Supplement* 64 (1978) 346–367.
- [49] G. I. Sivashinsky, Nonlinear analysis of hydrodynamic instability in laminar flames—i. derivation of basic equations, *Acta astronautica* 4 (11) (1977) 1177–1206.
- [50] S. Lee, M. Kooshkbaghi, K. Spiliotis, C. I. Siettos, I. G. Kevrekidis, Coarse-scale pdes from fine-scale observations via machine learning, *Chaos: An Interdisciplinary Journal of Nonlinear Science* 30 (1) (2020).
- [51] I. V. Karlin, S. Ansumali, C. E. Frouzakis, S. S. Chikatamarla, Elements of the lattice boltzmann method i: Linear advection equation, *Commun. Comput. Phys* 1 (4) (2006) 616–655.
- [52] H. Montanelli, N. Bootland, Solving periodic semilinear stiff pdes in 1d, 2d and 3d with exponential integrators, *Mathematics and Computers in Simulation* 178 (2020) 307–327.
- [53] P. Cvitanović, R. L. Davidchack, E. Siminos, On the state space geometry of the kuramoto–sivashinsky flow in a periodic domain, *SIAM Journal on Applied Dynamical Systems* 9 (1) (2010) 1–33.
- [54] P. Vincent, H. Larochelle, Y. Bengio, P.-A. Manzagol, Extracting and composing robust features with denoising autoencoders, in: *Proceedings of the 25th international conference on Machine learning*, 2008, pp. 1096–1103.
- [55] D. P. Kingma, J. Ba, Adam: A method for stochastic optimization, *arXiv preprint arXiv:1412.6980* (2014).
- [56] J. Xie, R. Girshick, A. Farhadi, Unsupervised deep embedding for clustering analysis, in: *International conference on machine learning*, PMLR, 2016, pp. 478–487.
- [57] M. Kamb, E. Kaiser, S. L. Brunton, J. N. Kutz, Time-delay observables for koopman: Theory and applications, *SIAM Journal on Applied Dynamical Systems* 19 (2) (2020) 886–917.
- [58] S. Pan, K. Duraisamy, On the structure of time-delay embedding in linear models of non-linear dynamical systems, *Chaos: An Interdisciplinary Journal of Nonlinear Science* 30 (7) (2020).

## A. Hyperparameters for L-HITS method

Table 5: Various hyper-parameters for the FHN model

Parameters	Values
Spatial dimension $n$	202
Temporal dimension $T$	5120
Time step $\Delta t$	0.01
Latent dimensions $z$	1, <b>2</b> , 4, 6, 8, 10
AE architecture	100: 100: 100: $z$ : 100: 100: 100
No. of epochs for training AE models	5000
Activation function	ReLU
Batch size	32
Learning rate	$1e - 03$
No. of epochs for training ResNet models	20000
Step sizes for ResNet models	$\Delta t$ , <b>2<math>\Delta t</math></b> , <b>4<math>\Delta t</math></b> , <b>8<math>\Delta t</math></b> , <b>16<math>\Delta t</math></b> , <b>32<math>\Delta t</math></b> , 64 $\Delta t$ , 128 $\Delta t$ , 256 $\Delta t$ , 512 $\Delta t$ , 1024 $\Delta t$
ResNet architecture	128: 128: 128: 128: 128: 128
Training data size	$4 \times 5120 \times 202$
Validation data size	$1 \times 5120 \times 202$
Testing data size	$1 \times 5120 \times 202$

Table 6: Various hyper-parameters used for the 1D KS equation

Parameters	Values
Spatial dimension $n$	120
Temporal dimension $T$	5121
Time step $\Delta t$	0.05
Latent dimensions $z$	1, 2, 4, 6, <b>8</b> , 10
AE architecture	120: 120: 100: $z$ : 100: 120: 120
No. of epochs for training AE models	5000
Activation function	ReLU
Batch size	32
Learning rate	$1e - 03$
No. of epochs for training ResNet models	20000
Step sizes for ResNet models	$\Delta t$ , 2 $\Delta t$ , 4 $\Delta t$ , <b>8<math>\Delta t</math></b> , <b>16<math>\Delta t</math></b> , <b>32<math>\Delta t</math></b> , <b>64<math>\Delta t</math></b> , 128 $\Delta t$ , 256 $\Delta t$ , 512 $\Delta t$ , 1024 $\Delta t$
ResNet architecture	1024: 1024: 1024
Training data size	$10 \times 5121 \times 120$
Validation data size	$5 \times 5121 \times 120$
Testing data size	$5 \times 5121 \times 120$